Since January 2020 Elsevier has created a COVID-19 resource centre with free information in English and Mandarin on the novel coronavirus COVID-19. The COVID-19 resource centre is hosted on Elsevier Connect, the company's public news and information website.

Elsevier hereby grants permission to make all its COVID-19-related research that is available on the COVID-19 resource centre - including this research content - immediately available in PubMed Central and other publicly funded repositories, such as the WHO COVID database with rights for unrestricted research re-use and analyses in any form or by any means with acknowledgement of the original source. These permissions are granted for free by Elsevier for as long as the COVID-19 resource centre remains active.

Article

Cell

Ebola Viral Glycoprotein Bound to Its Endosomal Receptor Niemann-Pick C1

Graphical Abstract

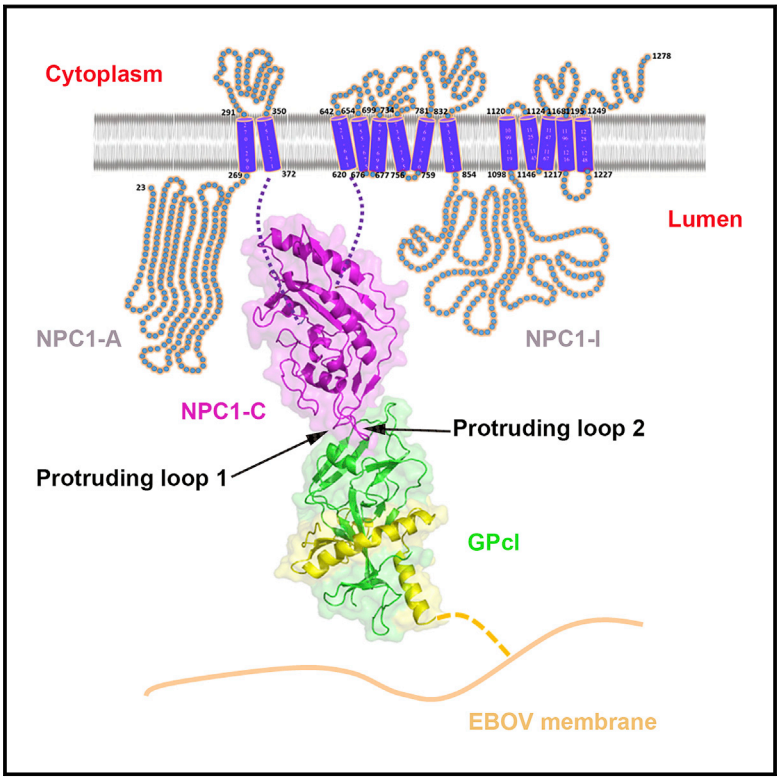

Authors

Han Wang, Yi Shi, Jian Song, Jianxun Qi, Guangwen Lu, Jinghua Yan, George F. Gao

Correspondence

gaof@im.ac.cn

In Brief

The crystal structure of the primed Ebola virus glycoprotein in complex with domain C of the endosomal entry receptor Niemann-Pick C1 reveals structural insights into filovirus fusion to the late endosome and the molecular basis for designing therapeutic inhibitors of viral entry.

Highlights

- Structural basis of Ebola virus endosomal-receptor binding
- NPC1 domain C (NPC1-C) displays a helical core structure with two protruding loops
- NPC1-C binds to the primed Ebola virus GP (GPcl) protein with a low affinity
- NPC1-C utilizes two protruding loops to engage a hydrophobic cavity on head of GPcl

Accession Numbers

5F18
5F1B

Wang et al., 2016, Cell *164*, 258–268
January 14, 2016 ©2016 Elsevier Inc.
http://dx.doi.org/10.1016/j.cell.2015.12.044

CellPress

Cell

Article

Ebola Viral Glycoprotein Bound to Its Endosomal Receptor Niemann-Pick C1

Han Wang,[1,3,10] Yi Shi,[1,2,3,4,5,10] Jian Song,[1,3,10] Jianxun Qi,[1,3,10] Guangwen Lu,[1,6] Jinghua Yan,[1,3,5,7] and George F. Gao[1,2,3,4,5,8,9,*]

[1]CAS Key Laboratory of Pathogenic Microbiology and Immunology, Institute of Microbiology, Chinese Academy of Sciences, Beijing 100101, China

[2]Research Network of Immunity and Health (RNIH), Beijing Institutes of Life Science, Chinese Academy of Sciences, Beijing 100101, China

[3]University of Chinese Academy of Sciences, Beijing 100049, China

[4]Center for Influenza Research and Early-warning, Chinese Academy of Sciences, Beijing 100101, China

[5]Shenzhen Key Laboratory of Pathogen and Immunity, Shenzhen Third People's Hospital, Shenzhen 518112, China

[6]West China Hospital Emergency Department (WCHED), State Key Laboratory of Biotherapy, West China Hospital, Sichuan University, and Collaborative Innovation Center of Biotherapy, Chengdu, Sichuan 610041, China

[7]CAS Key Laboratory of Microbial Physiology and Engineering, Institute of Microbiology, Chinese Academy of Sciences, Beijing 100101, China

[8]Collaborative Innovation Center for Diagnosis and Treatment of Infectious Diseases, Hangzhou 310003, China

[9]National Institute for Viral Disease Control and Prevention, Chinese Center for Disease Control and Prevention (China CDC), Beijing 102206, China

[10]Co-first author

*Correspondence: gaof@im.ac.cn

http://dx.doi.org/10.1016/j.cell.2015.12.044

SUMMARY

Filoviruses, including Ebola and Marburg, cause fatal hemorrhagic fever in humans and primates. Understanding how these viruses enter host cells could help to develop effective therapeutics. An endosomal protein, Niemann-Pick C1 (NPC1), has been identified as a necessary entry receptor for this process, and priming of the viral glycoprotein (GP) to a fusion-competent state is a prerequisite for NPC1 binding. Here, we have determined the crystal structure of the primed GP (GPcl) of Ebola virus bound to domain C of NPC1 (NPC1-C) at a resolution of 2.3 Å. NPC1-C utilizes two protruding loops to engage a hydrophobic cavity on head of GPcl. Upon enzymatic cleavage and NPC1-C binding, conformational change in the GPcl further affects the state of the internal fusion loop, triggering membrane fusion. Our data therefore provide structural insights into filovirus entry in the late endosome and the molecular basis for design of therapeutic inhibitors of viral entry.

INTRODUCTION

The filovirus family *Filoviradae*, including the genera *Ebolavirus* and *Marburgvirus*, can cause a rapidly lethal hemorrhagic fever in humans, and at present, no clinically approved antiviral therapeutics are available. Since 1967, Marburg virus has emerged multiple times, with modern strains showing greater mortality (Geisbert et al., 2007; Malherbe and Strickland-Cholmley, 1968; Siegert et al., 1968; Towner et al., 2006). The *Ebolavirus* consists of five recognized species, including Zaire, Sudan, Reston, Bundibugyo and Tai Forest viruses, four of which (except the Reston virus) can infect humans (Kuhn et al., 2013; Kuhn and Jahrling, 2010). Among these filoviruses, Ebola virus (EBOV) and the Marburgvirus (MARV) Angola variant cause the most severe diseases, with case fatality rates reaching ~90% (Feldmann and Geisbert, 2011; Sullivan et al., 2009). Recently, since December 2013, a historically unprecedented EBOV outbreak has occurred in the West Africa, causing more than 25,000 human infections and over 10,000 related deaths as of May 18th, 2015. Under this urgent situation, we are called for great efforts to develop the vaccines and antiviral therapeutics, which needs a comprehensive and decent understanding of the pathogenesis and molecular basis of EBOV infection.

Regarding the infection by filoviruses, including EBOV, the primarily infected cells are macrophages and dendritic cells. But the viruses exhibit a much broader cell tropism and can infect, upon primary infection, most of the cell types, including epithelial and non-epithelial cells, with the exception of lymphocytes and other non-adherent cells (Dube et al., 2010). Host cell attachment factors such as C-type lectins, including DC-SIGN (dendritic-cell-specific ICAM3-grabbing non-integrin; also known as CD209) and L-SIGN (liver and lymph node SIGN; also known as CLEC4M) and several cell-surface proteins such as integrins, T cell immunoglobulin and mucin domain-containing (TIM) proteins, and tyrosine protein kinase receptor 3 (TYRO3) family members have been shown to mediate the entry of filoviruses on the cell surface (Alvarez et al., 2002; Jemielity et al., 2013; Kondratowicz et al., 2011; Shimojima et al., 2007; Simmons et al., 2003; Takada et al., 2000, 2004; Wang et al., 2015). These attachment factors, however, do not function as authentic entry receptors (Brindley et al., 2011; Schornberg et al., 2009). Following binding to the cell surface, filoviruses are internalized by a macropinocytosis-like process and subsequently trafficked through early and late endosomes (Mulherkar et al., 2011; Nanbo

CrossMark

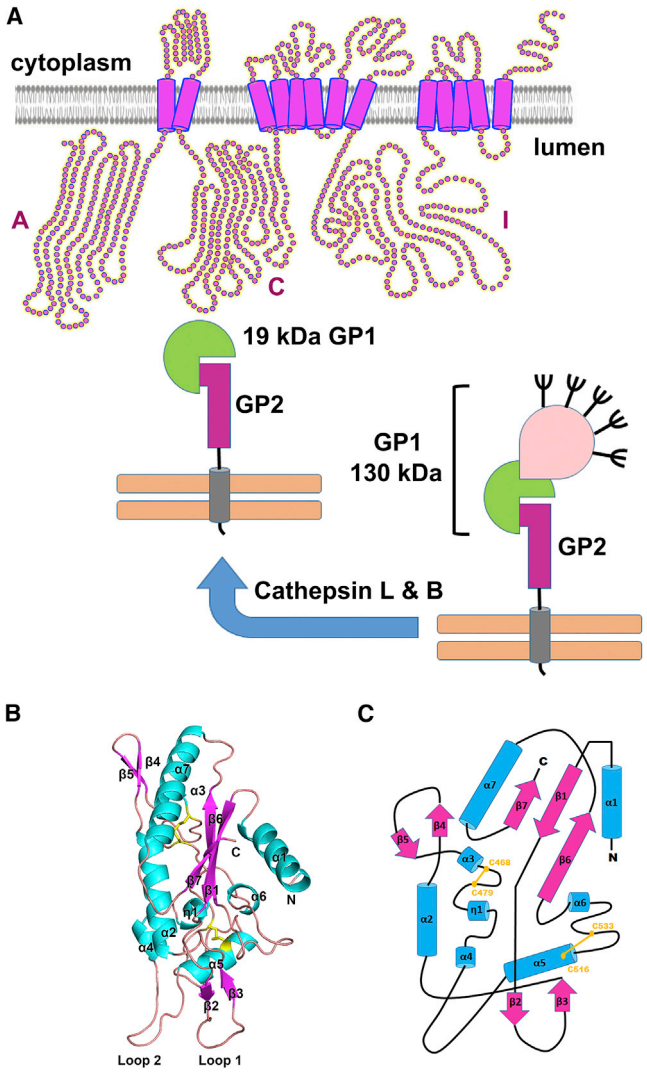

Figure 1. Model of NPC1 Bound to the Primed EBOV GP and Overall Structure of NPC1-C

(A) The full-length EBOV GP was primed by cathepsin L and B in the late endosome, and the highly glycosylated 130 kDa GP1 subunit was cleaved into a 19 kDa GP1, generating a primed form of GP (GPcl). Then, the GPcl binds to the domain C of NPC1 molecule (NPC1-C), which is an endosomal 13-transmembrane protein with three large luminal domains (domains A, C, and I).

(B) Crystal structure of NPC1-C. The helices (α and η) are colored in cyan, the β strands are colored in magenta, and the loops are colored in light pink. The disulfide bonds are colored in yellow. NPC1-C displays a helical core structure surrounded by several β strands with two extended loops.

(C) Topological secondary structure of NPC1-C. Secondary elements are shown as cylinders and arrows for helices and β strands.

See also Figures S1, S2, and S3 and Table S1.

et al., 2010; Saeed et al., 2010). The viral genome then penetrates into the cytoplasm after fusion of the viral envelope with the membrane of the late endosome. In the cytoplasm, the viral genome is replicated and transcribed, and new viral proteins are synthesized to assemble progeny virions, which bud from the cell surface (Bharat et al., 2011; Feldmann et al., 2013). Given its place at the initial step of virus infection, the entry process represents an ideal target for antiviral intervention: stopping the virus before it enters the cell.

The trimeric glycoprotein (GP) spike on the envelope of filoviruses mediates all stages of virus entry, including attachment, entry, and fusion (Lee and Saphire, 2009). Like all the other Class I viral fusion proteins, the EBOV GP is synthesized as a single polypeptide that is subsequently cleaved by furin-like proteases into GP1 and GP2 subunits, which remain together through an inter-subunit disulfide bond and non-covalent interactions. In contrast to other Class I viral fusion proteins, however, the simple furin cleavage event is not sufficient to prime EBOV GP (Neumann et al., 2007; Wool-Lewis and Bates, 1999). After entering into the cell, the virus is eventually trafficked to late endosomes, where GP is further primed to remove some "cap" components, thereby triggering the induction of the crucial membrane fusion event, which leads to viral penetration. The functional EBOV GP priming is mediated by the cysteine proteases cathepsin B and cathepsin L (Chandran et al., 2005; Schornberg et al., 2006), which cleave GP1 within the β13-β14 loop (Dube et al., 2009; Hood et al., 2010; Lee et al., 2008). Cathepsin cleavage removes ~60% of the amino acids from GP1, including the mucin-like domain, the glycan cap, and the outmost β strand of the proposed receptor binding region (Dube et al., 2009; Lee et al., 2008), resulting in a primed form of GP (named GPcl, the 19 kDa GP1 plus GP2) (Figure 1A). Unlike the full-length GP, the primed GPcl could bind to an endosomal membrane protein Niemann-Pick C1 (NPC1) (Miller et al., 2012), which is an indispensable host entry factor for EBOV infection (Carette et al., 2011; Côté et al., 2011). NPC1 is a ubiquitously expressed protein with multiple transmembrane domains and resides primarily in the limiting membranes of late endosomes and lysosomes (Carstea et al., 1997; Davies and Ioannou, 2000). It functions to aid cholesterol egress out of late endosomes for re-distribution to cellular membranes (including endoplasmic reticulum and plasma membrane) in the assistance of a soluble NPC2 protein (Sleat et al., 2004). Further studies have revealed that the second luminal domain (Domain C) of NPC1 (NPC1-C) is responsible for the binding to GPcl (Figure 1A) (Miller et al., 2012). However, how GPcl binds to NPC1 remains elusive, and structural study should be carried out to investigate the molecular features of the binding interface, which will guide further development of small antiviral molecules and antibodies for prevention and/or treatment of EBOV infection.

Here, we have determined the crystal structures of free NPC1-C and its complex with GPcl. The results revealed that NPC1-C displays a helical structure core surrounded by several β strands and contains two extended loops protruding outward for ligand interactions. Further GPcl/NPC1-C complex structure indeed shows that NPC1-C utilizes the two protruding loops to engage a hydrophobic cavity on the head of GPcl. Despite a low affinity between NPC1-C and GPcl as revealed by the biophysical analyses, upon enzymatic cleavage and NPC1-C binding, several conformational changes are shown to be induced in GPcl. After conformational changes, the uplift of the short 3_{10} helix in the β3-α1 loop likely helps to release the N-terminal portion of the internal fusion loop (IFL), thereby triggering the membrane fusion. The mutagenesis work in NPC1-C further confirmed that

the protruding loop 2 plays a more important role in the binding of NPC1-C to GPcl.

RESULTS

Structure of NPC1-C

The 1,278 residue human NPC1 contains 13 predicted transmembrane-spanning helices and 3 large luminal domains, domains A, C, and I (Figure 1A), the overall structural features of which remain to be illustrated. The crystal structure of the first luminal domain (domain A, also called N-terminal domain, NTD) is previously reported, showing a helical structural fold that contains a deep pocket for binding of sterols (Kwon et al., 2009). The structure information of the second and third luminal domains (domains C and I, respectively) of NPC1, however, are uncharacterized. Here, we used the *p*ET21a expression vector to produce human NPC1-C (residues 374 to 620) in *E. coli* BL21 (DE3), and the protein exists as insoluble inclusion bodies. Then the inclusion bodies were refolded to obtain soluble NPC1-C, which behaves as a single monomeric peak in gel filtration (Figure S1A). Some droplet-like crystals were obtained using the sitting drop vapor diffusion crystallization method, and the best crystal diffracted to a high resolution of 2.0 Å. As there is no homology structural model, the crystal structure of NPC1-C was determined by using single wavelength anomalous dispersion (SAD) phasing method with the help of a gold derivative. After several rounds of refinement, the final R_{free} and R_{work} reached 21.9 and 18.2, respectively (Table S1).

Overall, NPC1-C is mainly composed of seven α helices in the center as a core and seven β strands surrounding the core, with two protruding loops (Figure 1B). The first protruding loop (loop 1) is localized between β2 and β3 strands, while the second protruding loop (loop 2) is between α4 and α5 helices (Figure 1B). NPC1-C contains four cysteine residues, all of which were involved in forming disulfide bonds (C468-C479, C516-C533) (Figure 1C). Through analysis of primary protein sequence, NPC1-C has seven potential N-linked glycosylation sites, six of which locate in the loops, while one locates at the tip of α4 helix (Figure S1B). No glycans are observed in the crystal structure because the NPC1-C protein is expressed in bacterial cells that lack post-translational glycosylation modifications. However, the surface exposure of the seven sites indicates their accessibility for N-glyco-transferases.

The intact luminal NPC1-C consists of residues 372 to 640. In our crystal structure, only residues 384 to 624 are visible (Figure S2). We cannot see the electron density for the N-terminal 12 amino acids and C-terminal 16 amino acids (Figure S2), indicating that these regions might be flexible loops. It is assumed that, with these flexible N-terminal and C-terminal loops, the domain C can protrude from the endosomal membrane (Figure S3) and be easily bound by the primed GP molecule.

NPC1-C Bound to the GPcl with a Low Affinity

The mucin-deleted ectodomain of EBOV GP (GP-ectoΔmucin) was expressed in insect cells using baculovirus expression system and purified as a single homotrimeric peak by gel filtration (Figure S4A) following the previously reported method (Lee et al., 2008). Subsequently, thermolysin was used to cleave the GP-ecto protein to obtain GPcl, which also exists as a similar homotrimeric peak with relatively smaller size in the gel filtration (Figure S4A), following the previously developed method (Hashiguchi et al., 2015). The thermolysin, a protease that functions at neutral pH, can substitute for the cathepsin enzymes in priming GP (Schornberg et al., 2006). As expected, GP1 is cleaved into a 19 kDa protein moiety after thermolysin digestion (Figure S4A), resembling the version of GP component responsible for receptor binding in the endosome.

In order to test the active interactions between purified NPC1-C and GPcl proteins, we performed surface plasmon resonance (SPR) experiments to explore the binding affinity of these two proteins using a BIAcore 3000 instrument. The GP-ectoΔmucin or GPcl protein was immobilized on a CM5 chip, which was then flown through with the NPC1-C protein. Before we tested the NPC1-C protein, we first used 2G4 antibody (a member of the ZMapp cocktail (Qiu et al., 2014), which shows active binding capacity to the stem region of EBOV GP protein) as a positive control, confirming that the GP-ectoΔmucin and GPcl protein on the chip remain in the native prefusion state (Figure S4B). We found that 2G4 binds to GP-ectoΔmucin and GPcl protein with similar binding affinities (8.2 nM versus 3.8 nM) (Figure S4B). As expected, GP-ectoΔmucin does not bind to NPC1-C (Figure 2A), while GPcl binds to NPC1-C with a low affinity of 158 micromolar (μM) (Figures 2B and 2C). This binding affinity is much lower than that of some other highly pathogenic viruses such as MERS-CoV and SARS-CoV, which is among the nanomolar (nM) range (Lu et al., 2013).

In order to evaluate effect of the glycosylations in NPC1-C protein on binding of GPcl, we expressed glycosylated NPC1-C protein in 293T mammalian cells. This glycosylated NPC1-C protein exists as a dispersing band in the SDS-PAGE with an average molecular weight of about 55 kDa (Figure S5). Further SPR experiments revealed that the glycosylated NPC1-C does not bind to GP-ectoΔmucin (Figure 2D) but binds to GPcl with a comparable low affinity of 140 μM (Figures 2E and 2F) to the refolded NPC1-C protein (158 μM). It indicates that the glycosylations in NPC1-C have no effect on the binding of GPcl.

Complex Structure of NPC1-C and GPcl

The NPC1-C and GPcl were incubated together at a molar ratio of 1:1, and then crystallization screen was performed with the mixed protein complex. Initially, low-resolution-diffractive crystals were obtained, and after optimization of crystallization condition, a high-resolution-diffractive dataset was finally collected at the synchrotron facility. The complex structure was determined by molecular replacement at a resolution of 2.3 Å.

Structural analysis of the bound GPcl demonstrates that the cathepsin enzymes indeed cleave the GP protein within the β13-β14 loop (Figure 3A), and only residues 31 to 188 of GP1 subunit and residues 509 to 598 of GP2 subunit are visible in the crystal structure. After cathepsin cleavage, the glycan cap and mucin domain components would be removed (Figure 3A).

The solved complex structure reveals that NPC1-C binds the membrane-distal head of GPcl with a perpendicular angle (Figure 3B). NPC1-C mainly uses its two protruding loops to engage a hydrophobic cavity in the head of primed GP1 (Figure 3B). The hydrophobic cavity was formed by residues from the α1 helix, the

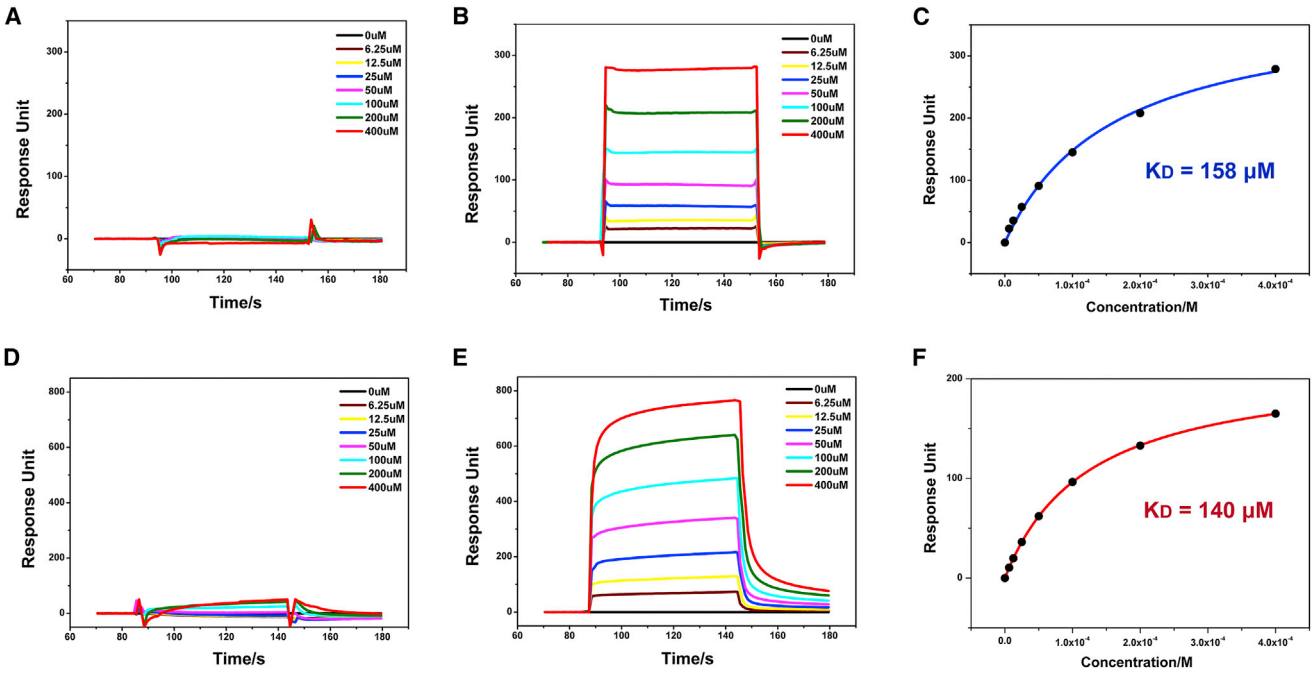

Figure 2. Binding Affinity of GPcl Bound to NPC1-C

(A) BIAcore diagram of refolded *E. coli*-expressed NPC1-C protein bound to the GP-ectoΔmucin protein. The refolded NPC1-C shows no binding to the GP-ectoΔmucin.

(B and C) BIAcore diagram and saturation curve of refolded NPC1-C protein bound to the GPcl protein. The refolded NPC1-C binds to the GPcl with a low affinity and a fast kinetics.

(D) BIAcore diagram of glycosylated 293T-expressed NPC1-C protein bound to the GP-ectoΔmucin protein. The glycosylated NPC1-C also shows no binding to the GP-ectoΔmucin.

(E and F) BIAcore diagram and saturation curve of glycosylated NPC1-C protein bound to the GPcl protein. The glycosylated NPC1-C binds to the GPcl with a similar low affinity and a fast kinetics. Response units were plotted against protein concentrations. The K_D values were calculated by the BIAcore 3000 analysis software (BIAevaluation Version 4.1).

See also Figures S4 and S5.

β4, β7, β9, and β10 strands, and the β9-β10 and β12-β13 loops (Figure 3B). The protruding loop 1 of NPC1-C contacts one side of the cavity, while the protruding loop 2 inserts into the cavity (Figure 3B). In the protruding loop 1, seven residues (Y420, Q421, Y423, P424, S425, G426, and D428) are involved in the interaction (Figure 3C, top), among which residues Y423 and P424 contribute most of the atom-to-atom contacts (Table 1). In the protruding loop 2, six residues (D501, D502, F503, F504, V505, and Y506) participate in the binding process (Figure 3C, top), and residues F503, F504, and Y506 play the major role by contributing the majority of the tight hydrophobic interactions with the head cavity of GPcl (Table 1). Moreover, residue D501 of NPC1-C forms a hydrogen bond with residue T83 of GPcl in the cavity (Figure 3C and Table 1). Reciprocally, the hydrophobic cavity of GPcl consists of residues V79, P80, T83, W86, G87, F88, L111, E112, I113, V141, G145, P146, C147, A152, and I170, while the other residues of K114, G118, S142, G143, and T144 form a hydrophilic patch contacting the protruding loop 1 with polar interactions (Figure 3C, bottom). Of these polar contacts, the NPC1-C residue Q421 forms a hydrogen bond with the GPcl residue T144, and the NPC1-C residue D428 could form a potential salt bridge with GPcl residue K114 in the hydrophilic patch (Figure 3C and Table 1).

Structural Comparison between GP and GPcl

Before GP is cleaved by the cathepsin enzymes, the binding site for NPC1-C is shielded by the glycan cap (Figure 4A). The β14 strand forms a hydrogen bond network with the β9 strand, and two aromatic residues F225 and Y232 insert into the hydrophobic cavity in the head of GPcl. By contrast, NPC1-C takes advantage of four aromatic residues (Y423, F503, F504, and Y506) and one hydrophobic residue P424 to interact with the hydrophobic cavity. Of special importance, residue F503 inserts into the cavity at a deeper position (Figure 4B). Thus, the binding of NPC1-C mimics the interaction between the glycan cap and the cavity but likely with a better binding capacity by providing more aromatic residues. Interestingly, a recent study revealed that a similar hydrophobic cavity is found in the primed Marburg virus GP protein, and the cavity can be targeted by a neutralizing antibody MR78 (Hashiguchi et al., 2015). MR78 binds to the cavity mainly through two aromatic residues F111.2 and Y112.2 (Figure 4C), with a similar hydrophobic interaction in the binding of NPC1-C to GPcl.

Through comparison between the unbound GP and the NPC1-C-bound GPcl, several conformational changes are observed. Two most dominant changes occur in the binding site of NPC1-C, including the β7-β8 loop and the α1 helix. In reference

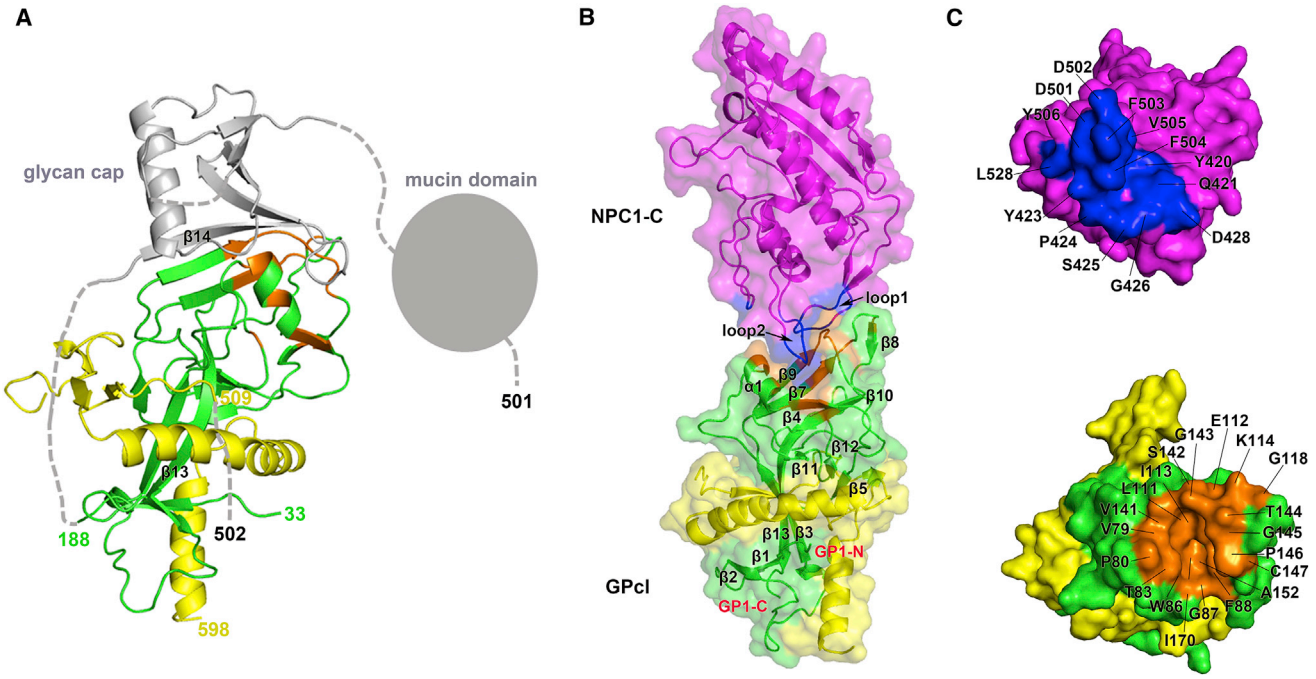

Figure 3. Complex Structure of NPC1-C Bound to GPcl

(A) The bound GPcl structure. The visible portions of GP1 and GP2 subunits are colored in green and yellow, respectively, and the other invisible or cleavage-removed portions are colored in gray.

(B) Overall complex structure. The NPC1-C uses its two protruding loops to bind to the head of GPcl at a perpendicular angle.

(C) Surface representations of interacting residues in the NPC1-C and GPcl. The residues responsible for the binding in the NPC1-C (top) are colored in blue, and the interacting residues in the GPcl (bottom) are colored in orange. The NPC1-C mainly utilizes aromatic residues to engage the cavity of the GPcl, which mainly consists of hydrophobic residues.

See also Table S1.

to that in the unbound GP, the β7-β8 loop moves downward, whereas the α1 helix goes upward upon engagement with NPC1-C (Figure 5A). With the movement of the α1 helix, the short 3^{10} helix in the β3-α1 loop raises upward correspondingly (Figure 5A). In the unbound GP, residue N73 in the beta turn forms a hydrogen bond with the main-chain carboxyl oxygen of residue K510, which is in the N-terminal portion of the internal fusion loop (IFL) (Figure 5B). The interaction can compromise the electric repulsion between K510 and R559 (in the HR1 helix of GP2) (Figure 5B). In the bound GPcl, due to the uplift of the short 3^{10} helix, residue N73 does not interact with residue K510, and the side chain of K510 points inward and easily generates an electric repulsion with residue R559 (Figure 5C). The unfavorable interaction likely helps to release the IFL and therefore make ready to trigger the membrane fusion in the late endosomes.

Mutagenesis Confirms the Key Interaction Residues

In order to clarify the interactions between the NPC1-C and GPcl, we performed mutagenesis work with NPC1-C and used the SPR experiment to test the binding. The structural analyses in the above section revealed that residues Y423, P424, F503, F504, and Y506 play the major role by contributing most of the interactions. Thus, we substituted these five sites with alanine (A) or glycine (G) residues, including quintuple substitution, double substitution (Y423&P424 or F503&F504), and single substitution. Unfortunately, the quintuple-A mutant (Y423A&P424A&F503A&F504A&Y506A), double mutant (Y423A&P424A), and two of the single mutants (Y423G and Y506G) cannot be refolded (Figures S6 and S7). As expected, the quintuple-G substitution (Y423G&P424G&F503G&F504G&Y506G) in NPC1-C abolishes its binding to GPcl (Figure 6A). The double mutant in loop 1 (Y423G&P424G) dramatically reduces the binding affinity, and the double mutants (both F503A&F504A and F503G&F504G) abolish the binding (Figures 6B–6D). The single mutants in loop 2 (F503G, F504G, F503A, F504A, and Y506A) similarly abolish the binding to GPcl, as observed for the quintuple mutant (Figures 6E–6I). However, the single mutants in loop 1 (P424G, Y423A and P424A) can keep the binding capacity to GPcl but with slightly lower affinities (Figures 6J–6L), compared with the wild-type NPC1-C. Taken together, the mutagenesis work points out that the protruding loop 2 contributes more to the GPcl binding.

DISCUSSION

Virus-cell membrane fusion is the means by which all enveloped viruses, including devastating human pathogens such as filovirus, influenza virus, and human immunodeficiency virus (HIV), enter cells and initiate the life cycle of virus infection (Backovic and Rey, 2012). This membrane fusion process is executed by

Table 1. Interaction between GPcl and NPC1-C

GPcl	Contacts[a]	NPC1-C
V79	3, 2, 4	Y423, F504, Y506
P80	2, 19, 1	D501, Y506, L528
T83	7, 9, 3	D501, F503, Y506
W86	11	F503
G87	4	F503
F88	3, 14	D502, F503
L111	2, 3	F503, F504
E112	3	F504
I113	6, 6	F503, F504
K114	8, 1	Q421, D428
G118	1	Q421
V141	10, 5, 4	Y423, P424, F504
S142	6, 16, 8, 12, 3	Y423, P424, S425, G426, F504
G143	6, 1, 2, 4	Q421, Y423, G426, F504
T144	4, 13, 2, 5, 6	Y420, Q421, F503, F504, V505
G145	4, 2, 1	F503, F504, V505
P146	3, 5, 4	D501, D502, F503
C147	1	D502
A152	2	F503
I170	1	F503

[a]Numbers represent the number of atom-to-atom contacts between the GPcl residues and the NPC1-C residues, which were analyzed by the Contact program in CCP4 suite (the distance cutoff is 4.5 Å).

one or more viral envelope glycoproteins, including one that is generally defined as the fusion protein. As viral fusion proteins can mediate virus entry and genome release, leading to infection, they are increasingly exploited as targets for antiviral interventions (Harrison, 2015). The fusion can occur either on the cell plasma membrane or endosomal membrane (Harrison, 2015).

With major breakthroughs in our understanding of the proteins or protein complexes that mediate membrane fusion between enveloped viruses and their host cells, the fusion trigger can be classified into four major types: (1) interaction of the fusion protein with a cell-surface receptor; (2) sequential interactions with a cell-surface receptor and co-receptor/s; (3) exposure to low pH environment in endosomes after entering the cell by a general "swallow" process (e.g., endocytosis); and (4) sequential interactions with a cell-surface receptor followed by exposure to low pH environment in endosomes (White et al., 2008). After fusion trigger, the fusion protein would undergo a series of marked conformational changes (White et al., 2008). A key early event is the exposure of the fusion loop (or fusion peptide), which is otherwise either buried or fastened in the native fusion protein (Harrison, 2015; White et al., 2008). When the fusion loop or fusion peptide is released, it binds to the target membrane, forming a rod-shaped intermediate, which connects the viral and target membranes. Next, the fusion protein bends approximately in half by conformational changes and draws the viral and target membranes into close proximity, finally resulting in the two membranes to merge (Harrison, 2015; Wang et al., 2005; White et al., 2008).

It seems that EBOV fusion does not follow the above-mentioned four types of fusion-trigger manners, and the viral GP needs first to be primed inside the endosome, after entering the cell by cell-surface receptor or co-factor induction, to expose its endosome-receptor binding domain for its fusion trigger (White et al., 2008). There is an EBOV receptor residing in the endosome, and therefore a low pH environment is needed to facilitate conformational changes in the primed GP after its endosomal receptor binding (Brecher et al., 2012; Gregory et al., 2011; Schornberg et al., 2006). It has been identified that the endosome-residing NPC1 is the endosome-receptor to bind to the primed GP (Carette et al., 2011; Côté et al., 2011). It has been shown that GP is processed by cathepsin L and B to yield a primed GP (GPcl) for its full function to trigger the membrane fusion (Chandran et al., 2005; Schornberg et al., 2006). NPC1-C domain has been proposed to be the binding partner of the primed GP (Miller et al., 2012).

In this study, we present the structural evidence that NPC1-C indeed binds to the primed EBOV GP, and SPR experiments reveal that the binding affinity is low. Since the binding affinity between individual NPC1-C and the primed GP is low, an obvious question raised here would be how the primed GP can efficiently bind to the endosomal receptor NPC. We can see that there are two possibilities: either the confinement in the late endosomes makes the local concentration of NPC1 to be very high, in which case a dissociation constant in the order of 100 μM would be sufficient, or that additional domains of NPC1 also contribute to the binding affinity. These possibilities or beyond should be pursued in the future.

The receptor binding region for NPC1-C is mainly a hydrophobic cavity in the head of the primed GP and is contacted by the two protruding loops of NPC1-C. Upon enzymatic cleavage and NPC1-C binding, we have observed several conformational changes in the GPcl, of which the upward movement of a short 3_{10} helix in the β3-α1 loop likely helps to release the N-terminal portion of the IFL in the GP2 subunit, which is probably triggering the membrane fusion. As the crystal structure of free GPcl is not resolved yet, we do not know if it is cathepsin cleavage that induces a membrane-fusion-priming conformational change in GPcl or the binding of GPcl by NPC1-C. However, our data support the notion that there should be a fifth fusion triggering type, i.e., exposure to a low pH environment in the late endosome and interaction with an endosomal receptor. The Marburgvirus has a similar hydrophobic cavity in its head of the primed GP (Hashiguchi et al., 2015) and also needs NPC1 for viral fusion (Carette et al., 2011; Côté et al., 2011). This fusion-triggering mechanism likely represents a unique feature for all the filoviruses.

The structural data of the GPcl/NPC1-C complex have immediately pointed toward the development of therapeutic agents that target their binding interface as the strategies to treat infections by EBOV and other filoviruses. Previously, compounds have been found to potentially inhibit EBOV entry by targeting the NPC1 molecule (Côté et al., 2011). There are two classes of NPC1-interacting compounds that can hamper the filovirus entry and infection, typified by compound 3.47 and compound U18666A (Côté et al., 2011). The former compound was shown to competitively block the primed GP binding to the membrane (Côté et al., 2011), and according to our structural information,

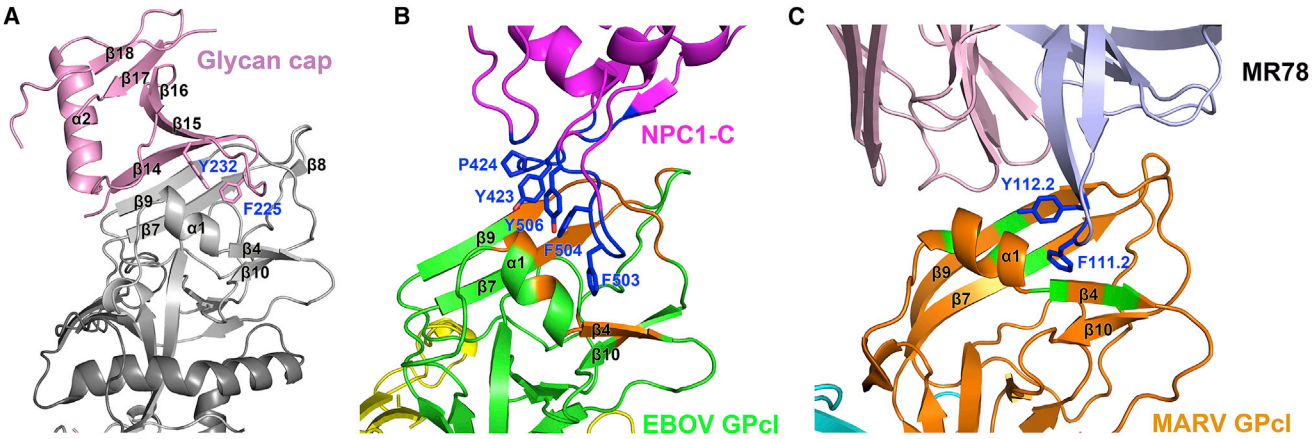

Figure 4. NPC1-C Mimics Similar but Stronger Interactions like the Glycan Cap in the Unprimed GP

(A) In the unprimed GP structure, the glycan cap utilizes two aromatic residues, F225 and Y232, to insert into the hydrophobic receptor binding cavity in the head of GPcl.

(B) NPC1-C takes advantage of four aromatic residues (Y423, F503, F504, and Y506) and one hydrophobic residue P424 to interact with the hydrophobic cavity. In particular, the residue F503 inserts into the cavity at a deeper position. Thus, the binding of NPC1-C mimics the interaction like the glycan cap but likely with a better binding capacity by providing more aromatic residues.

(C) An MARV-neutralizing antibody MR79 targets the hydrophobic binding cavity of MARV GP through aromatic residues (F111.2 and Y112.2).

this compound probably binds to the two protruding loops of NPC1-C, which should be explored in the future. By contrast, the latter compound cannot block the binding of primed GP to the NPC1-C but rather binding to a different site on NPC1 and causing endosomal calcium depletion, similar to other calcium channel inhibitors targeting the two-pore channels (TPCs) (Sakurai et al., 2015). A full-length structure of NPC1 molecule is ideal to illuminate the true nature of the molecular basis of these inhibitors' effect, which should be pursued in the future, though we solved the NPC1-C domain structure in this study. In addition to designing inhibitors targeting NPC1, our data also provide another important direction for inhibitor design. By targeting

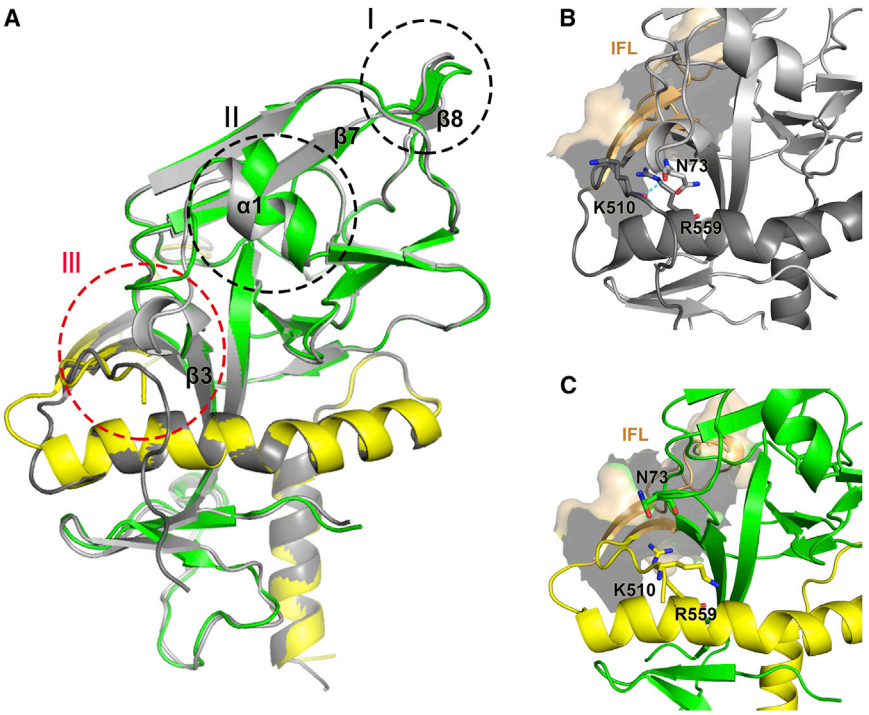

Figure 5. Conformational Changes in the GPcl upon Enzymatic Cleavage and NPC1-C Engagement

(A) Comparison of bound GPcl (GP1 in green and GP2 in yellow) and unbound GP-ectoΔmucin (gray glycan cap is not shown here). Three conformational changes are observed in the bound GPcl, including sites I, II, and III. At site I, the β7-β8 loop moves downward; at site II, the α1 helix raises upward. Accompanied with the raising α1 helix, an upward movement of the 3^{10} helix in the β3-α1 loop occurs at site III.

(B) Zoomed view of the site III in the unbound GP-ectoΔmucin. The residue N73 in the 3^{10} helix could form a hydrogen bond with the residue K510 in the N-terminal portion of the IFL. This interaction could separate the electric repulsion between K510 and R559 (in the HR1 helix of GP2).

(C) Zoomed view of the site III in the bound GPcl. The upward-moved residue N73 does not form a hydrogen bond with the residue K510, and the electric repulsion between the K510 and R539 may help to release the IFL and trigger the membrane fusion.

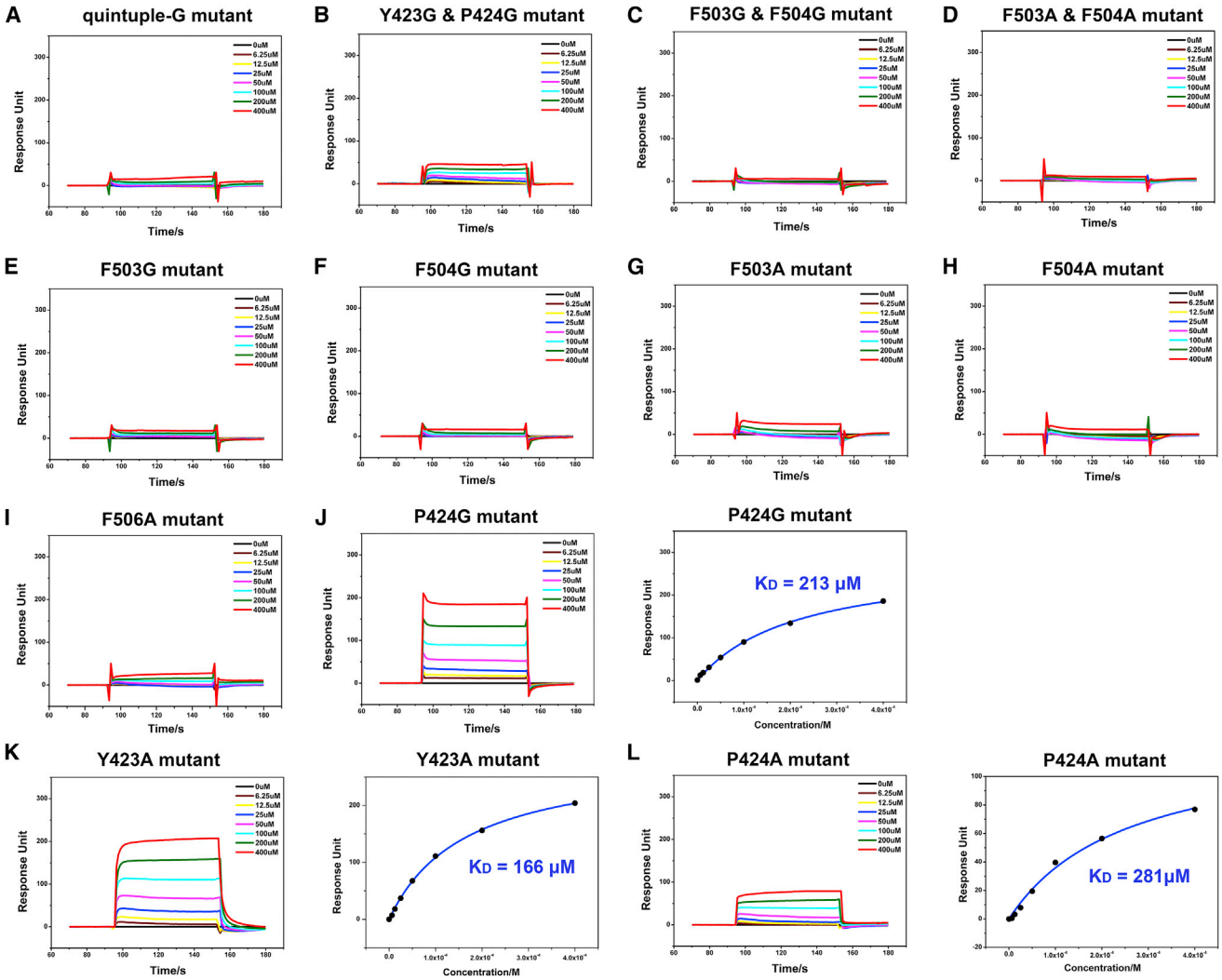

Figure 6. Alanine/Glycine-Scanning Mutagenesis Experiments on NPC1-C

(A–I) BIAcore diagrams of quintuple-G, Y423G&P424G, F503G&F504G, F503A&F504A, F503G, F504G, F503A, F504A, and Y506A mutants of NPC1-C binding to the GPcl. These nine mutants abolish the binding to the GPcl.

(J) BIAcore diagram and saturation curve of P424G mutant of NPC1-C binding to the GPcl. The P424G mutant can keep binding to the GPcl with an affinity of 213 μM, which is slightly lower than that of wild-type NPC1-C.

(K) BIAcore diagram and saturation curve of Y423A mutant of NPC1-C binding to the GPcl. The Y423A mutant can keep binding to the GPcl with an affinity of 166 μM, which is slightly lower than that of wild-type NPC1-C.

(L) BIAcore diagram and saturation curve of P424A mutant of NPC1-C binding to the GPcl. The P424A mutant can keep binding to the GPcl with an affinity of 281 μM, which is slightly lower than that of wild-type NPC1-C. Response units were plotted against protein concentrations. The K_D values were calculated by the BIAcore 3000 analysis software (BIAevaluation Version 4.1).

See also Figures S6 and S7.

the hydrophobic binding cavity in the head of the primed GP, some therapeutic agents, such as peptide inhibitors or small molecules, which can easily penetrate the cell membrane and reach the primed GP in the late endosomes, can be developed. Recently, a cross-reactive human antibody MR78 was identified to target this hydrophobic binding cavity of both MARV and EBOV (Hashiguchi et al., 2015). MR78 can neutralize the MARV but cannot neutralize the EBOV (Flyak et al., 2015), which might result from the fact that the hydrophobic binding cavity of MARV GP is partially exposed, whereas the cavity of EBOV GP is fully shielded by glycan cap before cathepsin cleavage in the endosome. The antibody cannot easily penetrate the cell membrane and reach the primed GP in the late endosomes, whereas the peptide inhibitors and small molecules can execute it. These previous studies, together with our study, provide a map by which therapy with cross-reactive antibodies and small inhibitors of entry could be developed. Otherwise, recent research advances in the nucleoprotein and its chaperoned VP35 protein also provide key targets for therapeutic intervention (Dong et al., 2015; Kirchdoerfer et al., 2015; Leung et al., 2015).

In conclusion, our results presented in this study for the structural basis of primed EBOV GP bound to its endosome-residing receptor NPC1 expand our understanding in the fusion trigger mechanism of enveloped viruses and provide valuable information for the design of therapeutics against infections by filoviruses.

EXPERIMENTAL PROCEDURES

Protein Production and Crystallization

The cDNAs encoding domain C residues 374–620 of NPC1 were cloned into pET21a vector with a C-terminal His_6-tag. The NPC1-C mutants were constructed by site-directed mutagenesis kit. The NPC1 domain C proteins (NPC1-C) were expressed in *Escherichia coli* strain BL21 (DE3) as inclusion bodies and then refolded in vitro using the method as previously described (Shi et al., 2011). The refolded NPC1-C proteins were then concentrated and purified by gel filtration on a HiLoad 16/60 Superdex 75 PG column (GE Healthcare). The fully glycosylated NPC1-C protein was expressed in 293T cells using the pCDNA4.0 vector and purified by metal affinity chromatography using a HisTrap HP 5 ml column (GE Healthcare) and then further purified by gel filtration on a HiLoad 16/60 Superdex 200 PG column (GE Healthcare). The EBOV transmembrane-and-mucin-domains-removed GP (GP-ectoΔmucin) protein was constructed as previously described (Lee et al., 2008) and expressed in baculovirus expression system using Sf9 cells (Shi et al., 2013; Stevens et al., 2004; Zhang et al., 2010). Soluble GP-ectoΔmucin protein was harvested from the culture supernatants by metal affinity chromatography and purified by gel filtration on a HiLoad 16/60 Superdex 200 PG column (GE Healthcare). To mimic endosomal protease cleavage and produce primed EBOV GP (GPcl), which was capable of NPC1 binding, 1 mg of EBOV GP-ectoΔmucin protein was incubated with 5 μg thermolysin overnight and purified on a Superdex 200 column.

All the crystals were obtained by using the sitting drop vapor diffusion method with 1 μl protein mixing with 1 μl reservoir solution. Diffractive crystals of free NPC1-C protein were obtained in a condition consisting of 0.07 M sodium acetate trihydrate (pH 4.6), 5.6% (w/v) polyethylene glycol 4,000, and 30% (v/v) glycerol at the protein concentration of 5 mg/ml. Derivative crystals were obtained by soaking NPC1-C crystals overnight in mother liquor containing 1 mM $KAuCl_4$.

To obtain the complex crystals of NPC1-C bound to GPcl, the individual proteins were in vitro mixed at a molar ratio of 1:1 and incubated at 4°C for about 2 hr before concentrating and being used for crystallization. The high-quality complex crystals were obtained in a reservoir solution of 15% (v/v) pentaerythritolpropoxylate, 0.2 M sodium chloride (pH 5.5), and 0.1 M MES-NaOH with a protein concentration of 10 mg/ml.

Data Collection and Structure Determination

For data collection, all crystals were cryo-protected by briefly soaking in reservoir solution supplemented with 20% (v/v) glycerol before flash-cooling in liquid nitrogen. All the datasets were processed with HKL2000 software (Otwinowski and Minor, 1997). The structure of NPC1-C was determined by the SAD method with anomalous signal method using Au derivative with SHELXD (Usón and Sheldrick, 1999) and Phaser (Read, 2001). The complex structure was solved by molecular replacement method using Phaser with the solved NPC1-C structure and previously reported GP structure (PDB code, 3CSY) as the search models. The atomic models were completed with Coot (Emsley and Cowtan, 2004) and refined with phenix.refine in Phenix (Adams et al., 2010), and the stereochemical qualities of the final models were assessed with PROCHECK (Laskowski et al., 1993). Data collection, processing, and refinement statistics are summarized in Table S1.

SPR Analysis

The SPR analysis was performed using a BIAcore 3000 machine with CM5 chips (GE Healthcare) at room temperature (25°C). All the proteins using in SPR analysis were exchanged to BIAcore buffer, consisting of 10 mM HEPES (pH 7.5), 150 mM NaCl, and 0.005% (v/v) Tween-20, via gel filtration. The WT and mutant NPC1-C proteins or antibody 2G4 were serially diluted to a serial of concentrations. The analytes were then used to flow over the chip surface with the response units measured. The binding kinetics was analyzed with the software BIAevaluation Version 4.1 using 1:1 Langmuir binding model.

ACCESSION NUMBERS

The crystal structures of NPC1-C and NPC1-C/GPcl complex have been submitted to Protein Data Bank with accession numbers PDB: 5F18 and PDB: 5F1B, respectively.

SUPPLEMENTAL INFORMATION

Supplemental Information includes Supplemental Experimental Procedures, seven figures, and one table and can be found with this article online at http://dx.doi.org/10.1016/j.cell.2015.12.044.

AUTHOR CONTRIBUTIONS

G.F.G. and Y.S. designed and supervised the study. H.W. and J.S. conducted the experiments. J.Q. collected the datasets and solved the structures. Y.S. and G.F.G. analyzed the data and wrote the manuscript. G.L. and J.Y. participated in the manuscript-editing and discussion.

ACKNOWLEDGMENTS

This work was supported by the special project of Ebola virus research from the President Foundation of Chinese Academy of Sciences (CAS), the National Natural Science Foundation of China (NSFC, Grant No. 81590761), Strategic Priority Research Program of the Chinese Academy of Sciences (XDB08020100), and China Ministry of Science and Technology National 973 Project (Grant numbers 2013CB531502 and 2014CB542503). We acknowledge Zheng Fan and Yiwei Liu for assistance with SPR experiments in Core Facility in Institute of Microbiology, CAS. We thank the staff of BL19U1 beamline at National Center for Protein Sciences Shanghai and Shanghai Synchrotron Radiation Facility (Shanghai, People's Republic of China) and BL17U beamline at Shanghai Synchrotron Radiation Facility for assistance during data collection. Xu Yang, Xiaoying Xu, Wenqian Duan, Yan Li, and Qihui Wang were involved in protein preparation and cell culture work during the revision stage of the manuscript. Y.S. is supported by the Excellent Young Scientist Program of the Chinese Academy of Sciences and the Youth Innovation Promotion Association CAS (2015078). G.F.G. is a leading principal investigator of the NSFC Innovative Research Group (Grant number 81321063).

Received: October 27, 2015
Revised: November 30, 2015
Accepted: December 23, 2015
Published: January 14, 2016

REFERENCES

Adams, P.D., Afonine, P.V., Bunkóczi, G., Chen, V.B., Davis, I.W., Echols, N., Headd, J.J., Hung, L.W., Kapral, G.J., Grosse-Kunstleve, R.W., et al. (2010). PHENIX: a comprehensive Python-based system for macromolecular structure solution. Acta Crystallogr. D Biol. Crystallogr. *66*, 213–221.

Alvarez, C.P., Lasala, F., Carrillo, J., Muñiz, O., Corbí, A.L., and Delgado, R. (2002). C-type lectins DC-SIGN and L-SIGN mediate cellular entry by Ebola virus in cis and in trans. J. Virol. *76*, 6841–6844.

Backovic, M., and Rey, F.A. (2012). Virus entry: old viruses, new receptors. Curr. Opin. Virol. *2*, 4–13.

Bharat, T.A., Riches, J.D., Kolesnikova, L., Welsch, S., Krähling, V., Davey, N., Parsy, M.L., Becker, S., and Briggs, J.A. (2011). Cryo-electron tomography of Marburg virus particles and their morphogenesis within infected cells. PLoS Biol. *9*, e1001196.

Brecher, M., Schornberg, K.L., Delos, S.E., Fusco, M.L., Saphire, E.O., and White, J.M. (2012). Cathepsin cleavage potentiates the Ebola virus

glycoprotein to undergo a subsequent fusion-relevant conformational change. J. Virol. *86*, 364–372.

Brindley, M.A., Hunt, C.L., Kondratowicz, A.S., Bowman, J., Sinn, P.L., McCray, P.B., Jr., Quinn, K., Weller, M.L., Chiorini, J.A., and Maury, W. (2011). Tyrosine kinase receptor Axl enhances entry of Zaire ebolavirus without direct interactions with the viral glycoprotein. Virology *415*, 83–94.

Carette, J.E., Raaben, M., Wong, A.C., Herbert, A.S., Obernosterer, G., Mulherkar, N., Kuehne, A.I., Kranzusch, P.J., Griffin, A.M., Ruthel, G., et al. (2011). Ebola virus entry requires the cholesterol transporter Niemann-Pick C1. Nature *477*, 340–343.

Carstea, E.D., Morris, J.A., Coleman, K.G., Loftus, S.K., Zhang, D., Cummings, C., Gu, J., Rosenfeld, M.A., Pavan, W.J., Krizman, D.B., et al. (1997). Niemann-Pick C1 disease gene: homology to mediators of cholesterol homeostasis. Science *277*, 228–231.

Chandran, K., Sullivan, N.J., Felbor, U., Whelan, S.P., and Cunningham, J.M. (2005). Endosomal proteolysis of the Ebola virus glycoprotein is necessary for infection. Science *308*, 1643–1645.

Côté, M., Misasi, J., Ren, T., Bruchez, A., Lee, K., Filone, C.M., Hensley, L., Li, Q., Ory, D., Chandran, K., and Cunningham, J. (2011). Small molecule inhibitors reveal Niemann-Pick C1 is essential for Ebola virus infection. Nature *477*, 344–348.

Davies, J.P., and Ioannou, Y.A. (2000). Topological analysis of Niemann-Pick C1 protein reveals that the membrane orientation of the putative sterol-sensing domain is identical to those of 3-hydroxy-3-methylglutaryl-CoA reductase and sterol regulatory element binding protein cleavage-activating protein. J. Biol. Chem. *275*, 24367–24374.

Dong, S., Yang, P., Li, G., Liu, B., Wang, W., Liu, X., Xia, B., Yang, C., Lou, Z., Guo, Y., and Rao, Z. (2015). Insight into the Ebola virus nucleocapsid assembly mechanism: crystal structure of Ebola virus nucleoprotein core domain at 1.8 Å resolution. Protein Cell *6*, 351–362.

Dube, D., Brecher, M.B., Delos, S.E., Rose, S.C., Park, E.W., Schornberg, K.L., Kuhn, J.H., and White, J.M. (2009). The primed ebolavirus glycoprotein (19-kilodalton GP1,2): sequence and residues critical for host cell binding. J. Virol. *83*, 2883–2891.

Dube, D., Schornberg, K.L., Shoemaker, C.J., Delos, S.E., Stantchev, T.S., Clouse, K.A., Broder, C.C., and White, J.M. (2010). Cell adhesion-dependent membrane trafficking of a binding partner for the ebolavirus glycoprotein is a determinant of viral entry. Proc. Natl. Acad. Sci. USA *107*, 16637–16642.

Emsley, P., and Cowtan, K. (2004). Coot: model-building tools for molecular graphics. Acta Crystallogr. D Biol. Crystallogr. *60*, 2126–2132.

Feldmann, H., and Geisbert, T.W. (2011). Ebola haemorrhagic fever. Lancet *377*, 849–862.

Feldmann, H., Sanchez, A., and Geisbert, T.W. (2013). Filoviridae: Marburg and Ebola Viruses. In Fields Vriology, D.M. Knipe and P.M. Howley, eds. (Philadelphia: Lippincott, Williams & Wilkins), pp. 923–956.

Flyak, A.I., Ilinykh, P.A., Murin, C.D., Garron, T., Shen, X., Fusco, M.L., Hashiguchi, T., Bornholdt, Z.A., Slaughter, J.C., Sapparapu, G., et al. (2015). Mechanism of human antibody-mediated neutralization of Marburg virus. Cell *160*, 893–903.

Geisbert, T.W., Daddario-DiCaprio, K.M., Geisbert, J.B., Young, H.A., Formenty, P., Fritz, E.A., Larsen, T., and Hensley, L.E. (2007). Marburg virus Angola infection of rhesus macaques: pathogenesis and treatment with recombinant nematode anticoagulant protein c2. J. Infect. Dis. *196* (*Suppl 2*), S372–S381.

Gregory, S.M., Harada, E., Liang, B., Delos, S.E., White, J.M., and Tamm, L.K. (2011). Structure and function of the complete internal fusion loop from Ebolavirus glycoprotein 2. Proc. Natl. Acad. Sci. USA *108*, 11211–11216.

Harrison, S.C. (2015). Viral membrane fusion. Virology *479-480*, 498–507.

Hashiguchi, T., Fusco, M.L., Bornholdt, Z.A., Lee, J.E., Flyak, A.I., Matsuoka, R., Kohda, D., Yanagi, Y., Hammel, M., Crowe, J.E., Jr., and Saphire, E.O. (2015). Structural basis for Marburg virus neutralization by a cross-reactive human antibody. Cell *160*, 904–912.

Hood, C.L., Abraham, J., Boyington, J.C., Leung, K., Kwong, P.D., and Nabel, G.J. (2010). Biochemical and structural characterization of cathepsin L-processed Ebola virus glycoprotein: implications for viral entry and immunogenicity. J. Virol. *84*, 2972–2982.

Jemielity, S., Wang, J.J., Chan, Y.K., Ahmed, A.A., Li, W., Monahan, S., Bu, X., Farzan, M., Freeman, G.J., Umetsu, D.T., et al. (2013). TIM-family proteins promote infection of multiple enveloped viruses through virion-associated phosphatidylserine. PLoS Pathog. *9*, e1003232.

Kirchdoerfer, R.N., Abelson, D.M., Li, S., Wood, M.R., and Saphire, E.O. (2015). Assembly of the Ebola Virus Nucleoprotein from a Chaperoned VP35 Complex. Cell Rep. *12*, 140–149.

Kondratowicz, A.S., Lennemann, N.J., Sinn, P.L., Davey, R.A., Hunt, C.L., Moller-Tank, S., Meyerholz, D.K., Rennert, P., Mullins, R.F., Brindley, M., et al. (2011). T-cell immunoglobulin and mucin domain 1 (TIM-1) is a receptor for Zaire Ebolavirus and Lake Victoria Marburgvirus. Proc. Natl. Acad. Sci. USA *108*, 8426–8431.

Kuhn, J.H., and Jahrling, P.B. (2010). Clarification and guidance on the proper usage of virus and virus species names. Arch. Virol. *155*, 445–453.

Kuhn, J.H., Bao, Y., Bavari, S., Becker, S., Bradfute, S., Brister, J.R., Bukreyev, A.A., Chandran, K., Davey, R.A., Dolnik, O., et al. (2013). Virus nomenclature below the species level: a standardized nomenclature for natural variants of viruses assigned to the family Filoviridae. Arch. Virol. *158*, 301–311.

Kwon, H.J., Abi-Mosleh, L., Wang, M.L., Deisenhofer, J., Goldstein, J.L., Brown, M.S., and Infante, R.E. (2009). Structure of N-terminal domain of NPC1 reveals distinct subdomains for binding and transfer of cholesterol. Cell *137*, 1213–1224.

Laskowski, R.A., Macarthur, M.W., Moss, D.S., and Thornton, J.M. (1993). Procheck - a program to check the stereochemical quality of protein structures. J. Appl. Cryst. *26*, 283–291.

Lee, J.E., and Saphire, E.O. (2009). Ebolavirus glycoprotein structure and mechanism of entry. Future Virol. *4*, 621–635.

Lee, J.E., Fusco, M.L., Hessell, A.J., Oswald, W.B., Burton, D.R., and Saphire, E.O. (2008). Structure of the Ebola virus glycoprotein bound to an antibody from a human survivor. Nature *454*, 177–182.

Leung, D.W., Borek, D., Luthra, P., Binning, J.M., Anantpadma, M., Liu, G., Harvey, I.B., Su, Z., Endlich-Frazier, A., Pan, J., et al. (2015). An Intrinsically Disordered Peptide from Ebola Virus VP35 Controls Viral RNA Synthesis by Modulating Nucleoprotein-RNA Interactions. Cell Rep. *11*, 376–389.

Lu, G., Hu, Y., Wang, Q., Qi, J., Gao, F., Li, Y., Zhang, Y., Zhang, W., Yuan, Y., Bao, J., et al. (2013). Molecular basis of binding between novel human coronavirus MERS-CoV and its receptor CD26. Nature *500*, 227–231.

Malherbe, H., and Strickland-Cholmley, M. (1968). Human disease from monkeys (Marburg virus). Lancet *1*, 1434.

Miller, E.H., Obernosterer, G., Raaben, M., Herbert, A.S., Deffieu, M.S., Krishnan, A., Ndungo, E., Sandesara, R.G., Carette, J.E., Kuehne, A.I., et al. (2012). Ebola virus entry requires the host-programmed recognition of an intracellular receptor. EMBO J. *31*, 1947–1960.

Mulherkar, N., Raaben, M., de la Torre, J.C., Whelan, S.P., and Chandran, K. (2011). The Ebola virus glycoprotein mediates entry via a non-classical dynamin-dependent macropinocytic pathway. Virology *419*, 72–83.

Nanbo, A., Imai, M., Watanabe, S., Noda, T., Takahashi, K., Neumann, G., Halfmann, P., and Kawaoka, Y. (2010). Ebolavirus is internalized into host cells via macropinocytosis in a viral glycoprotein-dependent manner. PLoS Pathog. *6*, e1001121.

Neumann, G., Geisbert, T.W., Ebihara, H., Geisbert, J.B., Daddario-DiCaprio, K.M., Feldmann, H., and Kawaoka, Y. (2007). Proteolytic processing of the Ebola virus glycoprotein is not critical for Ebola virus replication in nonhuman primates. J. Virol. *81*, 2995–2998.

Otwinowski, Z., and Minor, W. (1997). Processing of X-ray diffraction data collected in oscillation mode. Methods Enzymol. *276*, 307–326.

Qiu, X., Wong, G., Audet, J., Bello, A., Fernando, L., Alimonti, J.B., Fausther-Bovendo, H., Wei, H., Aviles, J., Hiatt, E., et al. (2014). Reversion of advanced Ebola virus disease in nonhuman primates with ZMapp. Nature *514*, 47–53.

Read, R.J. (2001). Pushing the boundaries of molecular replacement with maximum likelihood. Acta Crystallogr. D Biol. Crystallogr. *57*, 1373–1382.

Saeed, M.F., Kolokoltsov, A.A., Albrecht, T., and Davey, R.A. (2010). Cellular entry of ebola virus involves uptake by a macropinocytosis-like mechanism and subsequent trafficking through early and late endosomes. PLoS Pathog. *6*, e1001110.

Sakurai, Y., Kolokoltsov, A.A., Chen, C.C., Tidwell, M.W., Bauta, W.E., Klugbauer, N., Grimm, C., Wahl-Schott, C., Biel, M., and Davey, R.A. (2015). Ebola virus. Two-pore channels control Ebola virus host cell entry and are drug targets for disease treatment. Science *347*, 995–998.

Schornberg, K., Matsuyama, S., Kabsch, K., Delos, S., Bouton, A., and White, J. (2006). Role of endosomal cathepsins in entry mediated by the Ebola virus glycoprotein. J. Virol. *80*, 4174–4178.

Schornberg, K.L., Shoemaker, C.J., Dube, D., Abshire, M.Y., Delos, S.E., Bouton, A.H., and White, J.M. (2009). Alpha5beta1-integrin controls ebolavirus entry by regulating endosomal cathepsins. Proc. Natl. Acad. Sci. USA *106*, 8003–8008.

Shi, Y., Qi, J., Iwamoto, A., and Gao, G.F. (2011). Plasticity of human CD8αα binding to peptide-HLA-A*2402. Mol. Immunol. *48*, 2198–2202.

Shi, Y., Zhang, W., Wang, F., Qi, J., Wu, Y., Song, H., Gao, F., Bi, Y., Zhang, Y., Fan, Z., et al. (2013). Structures and receptor binding of hemagglutinins from human-infecting H7N9 influenza viruses. Science *342*, 243–247.

Shimojima, M., Ikeda, Y., and Kawaoka, Y. (2007). The mechanism of Axl-mediated Ebola virus infection. J. Infect. Dis. *196* (*Suppl 2*), S259–S263.

Siegert, R., Shu, H.L., and Slenczka, W. (1968). [Isolation and identification of the "Marburg virus"]. Dtsch. Med. Wochenschr. *93*, 604–612.

Simmons, G., Reeves, J.D., Grogan, C.C., Vandenberghe, L.H., Baribaud, F., Whitbeck, J.C., Burke, E., Buchmeier, M.J., Soilleux, E.J., Riley, J.L., et al. (2003). DC-SIGN and DC-SIGNR bind ebola glycoproteins and enhance infection of macrophages and endothelial cells. Virology *305*, 115–123.

Sleat, D.E., Wiseman, J.A., El-Banna, M., Price, S.M., Verot, L., Shen, M.M., Tint, G.S., Vanier, M.T., Walkley, S.U., and Lobel, P. (2004). Genetic evidence for nonredundant functional cooperativity between NPC1 and NPC2 in lipid transport. Proc. Natl. Acad. Sci. USA *101*, 5886–5891.

Stevens, J., Corper, A.L., Basler, C.F., Taubenberger, J.K., Palese, P., and Wilson, I.A. (2004). Structure of the uncleaved human H1 hemagglutinin from the extinct 1918 influenza virus. Science *303*, 1866–1870.

Sullivan, N.J., Martin, J.E., Graham, B.S., and Nabel, G.J. (2009). Correlates of protective immunity for Ebola vaccines: implications for regulatory approval by the animal rule. Nat. Rev. Microbiol. *7*, 393–400.

Takada, A., Watanabe, S., Ito, H., Okazaki, K., Kida, H., and Kawaoka, Y. (2000). Downregulation of beta1 integrins by Ebola virus glycoprotein: implication for virus entry. Virology *278*, 20–26.

Takada, A., Fujioka, K., Tsuiji, M., Morikawa, A., Higashi, N., Ebihara, H., Kobasa, D., Feldmann, H., Irimura, T., and Kawaoka, Y. (2004). Human macrophage C-type lectin specific for galactose and N-acetylgalactosamine promotes filovirus entry. J. Virol. *78*, 2943–2947.

Towner, J.S., Khristova, M.L., Sealy, T.K., Vincent, M.J., Erickson, B.R., Bawiec, D.A., Hartman, A.L., Comer, J.A., Zaki, S.R., Ströher, U., et al. (2006). Marburgvirus genomics and association with a large hemorrhagic fever outbreak in Angola. J. Virol. *80*, 6497–6516.

Usón, I., and Sheldrick, G.M. (1999). Advances in direct methods for protein crystallography. Curr. Opin. Struct. Biol. *9*, 643–648.

Wang, X.J., Bai, Y.D., Zhang, G.Z., Zhao, J.X., Wang, M., and Gao, G.F. (2005). Structure and function study of paramyxovirus fusion protein heptad repeat peptides. Arch. Biochem. Biophys. *436*, 316–322.

Wang, H., Qi, J., Liu, N., Li, Y., Gao, J., Zhang, T., Chai, Y., Gao, F., Zhang, H., Li, X., et al. (2015). Crystal structures of human TIM members: Ebolavirus entry-enhancing receptors. Chin. Sci. Bull. *60*, 3438–3453.

White, J.M., Delos, S.E., Brecher, M., and Schornberg, K. (2008). Structures and mechanisms of viral membrane fusion proteins: multiple variations on a common theme. Crit. Rev. Biochem. Mol. Biol. *43*, 189–219.

Wool-Lewis, R.J., and Bates, P. (1999). Endoproteolytic processing of the ebola virus envelope glycoprotein: cleavage is not required for function. J. Virol. *73*, 1419–1426.

Zhang, W., Qi, J., Shi, Y., Li, Q., Gao, F., Sun, Y., Lu, X., Lu, Q., Vavricka, C.J., Liu, D., et al. (2010). Crystal structure of the swine-origin A (H1N1)-2009 influenza A virus hemagglutinin (HA) reveals similar antigenicity to that of the 1918 pandemic virus. Protein Cell *1*, 459–467.